Earth and Planetary Science Letters 329–330 (2012) 109–121

Contents lists available at SciVerse ScienceDirect

Earth and Planetary Science Letters

journal homepage: www.elsevier.com/locate/epsl

The influence of magmatic differentiation on the oxidation state of Fe in a basaltic arc magma

Katherine A. Kelley [a,*], Elizabeth Cottrell [b]

[a] Graduate School of Oceanography, University of Rhode Island, Narragansett Bay Campus, Narragansett, RI 20882, USA
[b] Smithsonian Institution, National Museum of Natural History, Washington, DC 20560, USA

ARTICLE INFO

Article history:
Received 27 August 2011
Received in revised form 13 February 2012
Accepted 14 February 2012
Available online xxxx

Editor: R.W. Carlson

Keywords:
oxygen fugacity
XANES
melt Inclusions
subduction
volatiles
degassing

ABSTRACT

Subduction zone basalts are more oxidized than basalts from other tectonic settings (e.g., higher $Fe^{3+}/\sum Fe$), and this contrast may play a central role in the unique geochemical processes that generate arc and continental crust. The processes generating oxidized arc magmas, however, are poorly constrained, although they appear inherently linked to subduction. Near-surface differentiation processes unique to arc settings might drive oxidation of magmas that originate in equilibrium with a relatively reduced mantle source. Alternatively, arc magmas could record the oxidation conditions of a relatively oxidized mantle source. Here, we present new measurements of olivine-hosted melt inclusions from a single eruption of Agrigan volcano, Marianas, in order to test the influence of differentiation processes vs. source conditions on the $Fe^{3+}/\sum Fe$ ratio, a proxy for system oxygen fugacity (fO_2). We determined $Fe^{3+}/\sum Fe$ ratios in glass inclusions using μ-XANES and couple these data with major elements, dissolved volatiles, and trace elements. After correcting for post-entrapment crystallization, $Fe^{3+}/\sum Fe$ ratios in the Agrigan melt inclusions (0.219 to 0.282), and their modeled fO_2s (ΔQFM +1.0 to +1.8), are uniformly more oxidized than MORB, and preserve a portion of the evolution of this magma from 5.7 to 3.2 wt.% MgO. Fractionation of olivine ± clinopyroxene ± plagioclase should increase $Fe^{3+}/\sum Fe$ as MgO decreases in the melt, but the data show $Fe^{3+}/\sum Fe$ ratios decreasing as MgO decreases below 5 wt.% MgO. The major element trajectories, taken in combination with this strong reduction trend, are inconsistent with crystallization of common ferromagnesian phases found in the bulk Agrigan sample, including magnetite. Rather, decreasing $Fe^{3+}/\sum Fe$ ratios correlate with decreasing S concentrations, suggesting that electronic exchanges associated with SO_2 degassing may dominate $Fe^{3+}/\sum Fe$ variations in the melt during differentiation. In the case of this magma, the dominant effect of differentiation on magmatic fO_2 is reduction rather than oxidation. Tracing back Agrigan melts with MgO > 5 wt.% (i.e., minimally degassed for S) along a modeled olivine fractionation trend to primary melts in equilibrium with Fo_{90} olivine reveals melts in equilibrium with the mantle beneath Agrigan at fO_2s of ΔQFM +1 to +1.6, significantly more oxidized than current constraints for the mantle beneath mid-ocean ridges.

1. Introduction

The availability of oxygen to participate in chemical reactions within the Earth's mantle and magmatic systems (i.e., oxygen fugacity; fO_2) is a critical property that controls key igneous processes such as the speciation and partitioning of multi-valent elements, phase assemblages and equilibria, and the composition of volcanic gases. The ability of lavas erupted at the surface to preserve accurate records of the magmatic and source fO_2 they experienced in the Earth's deep interior, however, is a matter of significant debate (e.g., Ballhaus, 1993; Canil, 2002; Cottrell and Kelley, 2011; Kelley and Cottrell, 2009; Lee et al., 2005, 2010). The observation that basalts erupted at arc volcanoes are notably more oxidized than those erupted at mid-ocean ridges is generally uncontested (e.g., Ballhaus, 1993; Carmichael, 1991), but the cause of oxidation in the arc environment remains an open and important question. One hypothesis invokes oxidation of subduction zone mantle sources by oxidized fluids derived from subducted slabs (e.g., Brandon and Draper, 1996; Wood et al., 1990). The oxidation states of Fe in arc basalts have been quantitatively linked to tracers of slab additions (H_2O, Ba/La; Kelley and Cottrell, 2009) in support of this model. An alternate view, based on models of redox-sensitive element partitioning or isotope fractionation during mantle melting (e.g., Dauphas et al., 2009; Lee et al., 2005, 2010; Mallmann and O'Neill, 2009), suggests that mantle source fO_2 does not vary with tectonic setting, and that arc basalts must thus become oxidized as they differentiate along the path from the mantle source to the Earth's surface. Few studies have yet explicitly measured the effects of magmatic crystallization and degassing on the redox conditions of arc magmas.

* Corresponding author. Tel.: +1 401 874 6838; fax: +1 401 874 6811.
E-mail addresses: kelley@gso.uri.edu (K.A. Kelley), cottrelle@si.edu (E. Cottrell).

0012-821X/$ – see front matter © 2012 Elsevier B.V. All rights reserved.
doi:10.1016/j.epsl.2012.02.010

In theory, differentiation is a sensible process for accomplishing magmatic oxidation. Early-crystallizing mafic minerals (e.g., olivine, clinopyroxene) preferentially remove Fe^{2+} into lattice sites, thereby enriching the liquid in Fe^{3+} if the magma is closed to oxygen exchange with its surroundings. Mid-ocean ridge basalts (MORB) show small increases in $Fe^{3+}/\sum Fe$ ratio (i.e., $Fe^{3+}/[Fe^{2+}+Fe^{3+}]$) with decreasing MgO, consistent with closed-system removal of Fe^{2+} by the crystallizing phase assemblage (Cottrell and Kelley, 2011). In MORB magmas, $Fe^{3+}/\sum Fe$ ratios are observed and projected to increase by only 0.03 as MgO decreases from 10 to 5 wt.% (Cottrell and Kelley, 2011). This is clearly insufficient to explain the $Fe^{3+}/\sum Fe$ ratios observed in arc lavas. In MORB systems, H_2 degassing has also been proposed as a mechanism for "auto-oxidation" of lavas during eruption (Holloway, 2004), although at fO_2 relevant for MORB (e.g., conditions of the quartz–fayalite–magnetite buffer [QFM]) this process is too inefficient and self-limiting to drive resolvable changes in MORB fO_2 (Cottrell and Kelley, 2011). The differentiation paths of arc magmas, however, are significantly different from MORBs. Arc magmas are generally more volatile-rich, and when they erupt, they are on average more evolved and more degassed than MORBs. Yet, geochemical investigation of Mexican andesites and dacites indicates that crystallization and degassing cannot explain the elevated oxidation states of these magmas either (Crabtree and Lange, 2011). These observations warrant explicit attention to the unique case of arc basalts which, in an ocean–ocean convergent margin, offer the advantages of avoiding the potentially complicated passage through thick continental crust and provide magmas that are less differentiated from their mantle source. How do these magmas acquire their oxidized condition?

Here, we present a specific test of the alternate hypotheses of source vs. differentiation as the cause of oxidation in basaltic arc magmas by examining the magmatic redox conditions recorded during differentiation of a single arc magma. Using melt inclusions, trapped within olivine crystals over a period of time in the magmatic cooling history, this study captures a significant range of the liquid line of descent of one eruption of Agrigan volcano, Marianas, recording both the effects of magmatic degassing and crystallization processes on the composition and redox state of the magma.

2. Samples and methods

2.1. Geologic setting and samples

Agrigan volcano is located in the central island providence of the active Mariana island arc (see the electronic supplement). Trace element and isotopic signatures of Agrigan lavas indicate significant incorporation of subducted sediment into the mantle source beneath Agrigan, making it an important end-member composition among the Mariana islands (e.g., Elliott et al., 1997; Plank, 2005; Stern and Ito, 1983; Woodhead, 1988, 1989). Studies of naturally-glassy olivine-hosted melt inclusions from Agrigan also indicate high concentrations of dissolved H_2O in Agrigan magmas (~5 wt.%; Kelley et al., 2010; Shaw et al., 2008), which indicate a strong subduction component. These clear slab-derived geochemical signatures, and the absence of thick continental crust, make Agrigan an ideal place to conduct this test because the path from the subduction-influenced mantle wedge to the erupted tephra is more straightforward. The tephra sample selected for this study (AGR19-02) is rich in euhedral olivine phenocrysts that contain abundant glassy melt inclusions. Inclusions selected for preparation were naturally glassy with no visible secondary or synchronously trapped crystal phases, petrographically determined to be fully enclosed in the host olivine crystals, and contained either a single vapor bubble or no bubble.

2.2. Analytical methods

We analyzed glass inclusions and host olivines using a variety of micro-analytical methods to determine major and trace element composition of glasses and minerals, as well as dissolved volatile concentrations and $Fe^{3+}/\sum Fe$ ratios of glasses. At the Smithsonian Institution, electron microprobe analysis provided major element, S, and Cl data (Table 1) and Fourier transform infrared (FTIR) spectroscopy provided dissolved volatile concentrations (Table 1). We determined $Fe^{3+}/\sum Fe$ ratios of glass inclusions using micro X-ray absorption near-edge structure (μ-XANES) spectroscopy (Table 1; Cottrell et al., 2009) at beamline X26A of the National Synchrotron Light Source, Brookhaven National Lab, and $Fe^{3+}/\sum Fe$ of the whole rock at the Smithsonian Institution via micro-colorimetry (Cottrell and Kelley, 2011). Trace element concentrations were determined using laser-ablation inductively-coupled plasma mass spectrometry (LA-ICP-MS; Kelley et al., 2003) at the Graduate School of Oceanography, University of Rhode Island. Details on sample preparation, analytical procedures, and complete data tables are provided in the electronic supplement.

3. Results

3.1. Assessment of post-entrapment crystallization or modification

As a melt inclusion cools within its host olivine, some quantity of the host mineral may precipitate from the melt onto the inclusion walls after entrapment, and/or diffusive processes may drive exchanges of major elements between an inclusion and the evolving melt outside the host crystal. The melt inclusion data show remarkable consistency with whole-rock compositions from Agrigan over a range of MgO. Using the criteria of Danyushevsky et al. (2000), we find that post-entrapment diffusive re-equilibration or disequilibrium modification, specifically Fe^{2+} loss from the inclusions, was minimal (see the electronic supplement). We assess the extent to which post-entrapment crystallization (PEC) may have modified glass inclusion compositions by comparing the measured host olivine compositions to the equilibrium olivine compositions predicted by each melt inclusion, using $K_D^{ol/liq}(Fe^{2+}/Mg)=0.3$ (see the electronic supplement). In this case, the knowledge of the $Fe^{3+}/\sum Fe$ ratio of each glass inclusion offers a significant advantage, as this comparison is highly sensitive to small extents of PEC. The inclusions are hosted by a broad range of olivine compositions ($Fo_{82\text{-}73}$), and extents of PEC range from 0 to 3.3%. Many of the analyzed glass inclusions are in near-perfect Fe–Mg exchange equilibrium with their hosts, and we consider inclusions indicating <2% PEC as the most faithful records of the magma composition. These inclusions were corrected for PEC, if necessary, by assessing the olivine composition in equilibrium with each inclusion using $K_D^{ol/liq}(Fe^{2+}/Mg)=0.3$, then adding 0.1% of the equilibrium olivine back to the glass composition, and repeating these steps until equilibrium with the host olivine was reached, assuming the total moles of Fe^{3+} in each inclusion remained unchanged during these very minor extents of PEC (Table 1).

3.2. Fe speciation and oxygen fugacity of the Agrigan Magma

The $Fe^{3+}/\sum Fe$ ratios of the Agrigan glass inclusions, after correction for PEC, range from 0.219 to 0.282. These ratios are uniformly higher than in MORBs (0.16 ± 0.01; Cottrell and Kelley, 2011) and the back-arc basin basalts from the Mariana trough (0.15–0.19; Kelley and Cottrell, 2009), but overlap with the higher end of $Fe^{3+}/\sum Fe$ ratios reported for global arc basaltic melt inclusions (0.18–0.32) by Kelley and Cottrell (2009). This contrast is broadly consistent with past observations of whole-rock $Fe^{3+}/\sum Fe$ ratios of basalts from ridge and arc settings determined by wet chemistry, and spinel compositions from peridotites (e.g., Ballhaus, 1993; Carmichael, 1991; Christie et al., 1986; Parkinson and Arculus, 1999; Wood et

Table 1
Major element compositions and $Fe^{3+}/\sum Fe$ ratios of olivine-hosted glass inclusions and host olivines from Agrigan, Marianas.

Sample		AGR19-02																			
Inclusion #		01	02	03	04	05	07	08	09	10	11	12A[a]	12B	13	14	15	16	17	18	19	20
Glass inclusion																					
SiO_2	wt.%	46.73	46.68	53.47	47.00	48.41	47.19	47.92	48.41	46.13	46.92	51.54	46.64	47.99	46.49	46.27	46.00	49.68	48.36	47.40	48.36
TiO_2	wt.%	0.77	0.73	0.97	0.66	0.83	0.85	0.77	0.89	0.74	0.77	1.05	0.74	0.81	0.68	0.63	0.67	0.82	0.83	0.84	0.75
Al_2O_3	wt.%	16.79	17.86	16.23	17.68	16.24	18.71	16.52	16.99	18.09	17.93	17.96	18.31	16.98	17.53	18.17	17.28	16.89	16.48	18.78	16.83
FeO*	wt.%	10.30	8.58	9.29	9.50	9.87	9.33	9.83	10.12	8.99	9.10	7.98	10.18	10.30	9.83	9.45	10.67	8.70	9.67	8.35	8.69
FeO	wt.%	7.40	6.37	7.25	7.15	7.51	7.27	7.54	8.07	6.56	6.90	6.14	7.88	7.91	7.44	6.94	8.10	6.50	7.29	6.28	6.32
Fe_2O_3	wt.%	3.23	2.45	2.26	2.61	2.62	2.29	2.54	2.28	2.69	2.44	2.05	2.56	2.66	2.65	2.79	2.85	2.44	2.64	2.29	2.62
MnO	wt.%	0.20	0.21	0.17	0.26	0.27	0.17	0.20	0.23	0.15	0.21	0.18	0.23	0.23	0.18	0.21	0.22	0.18	0.20	0.19	0.18
MgO	wt.%	5.19	4.73	3.22	4.59	4.22	4.34	5.27	3.47	4.59	4.62	3.78	4.05	4.26	5.24	4.47	5.36	3.97	4.57	3.96	4.50
CaO	wt.%	12.30	13.28	8.36	12.79	11.65	12.66	12.24	11.90	12.64	12.42	10.18	12.61	11.27	11.66	13.50	12.07	10.79	11.35	13.08	12.31
Na_2O	wt.%	1.79	1.91	3.31	1.96	2.21	2.31	1.93	2.34	1.77	2.00	2.07	2.11	2.28	2.01	1.72	2.09	2.38	2.32	2.04	2.13
K_2O	wt.%	0.43	0.40	1.36	0.38	0.51	0.54	0.46	0.62	0.37	0.43	0.96	0.48	0.57	0.46	0.38	0.42	0.86	0.66	0.40	0.55
P_2O_5	wt.%	0.13	0.15	0.32	0.11	0.13	0.17	0.15	0.16	0.14	0.12	0.26	0.09	0.14	0.13	0.12	0.14	0.29	0.19	0.12	0.16
Total	wt.%	94.97	94.77	96.93	95.20	94.61	96.51	95.54	95.37	93.88	94.76	96.16	95.70	95.08	94.48	95.21	95.20	94.80	94.89	95.39	94.72
H_2O	wt.%	4.12	2.78	2.12	3.25	4.12	2.72	3.61	3.07	4.56	3.49	2.78	3.00	3.30	3.63	4.25	4.36	4.21	3.94	3.25	3.83
CO_2[b]	ppm	–	–	–	629	–	142	–	–	485	419	–	431	131	457	903	549	400	–	–	–
S	ppm	1474	1125	771	1170	813	1404	780	1050	1577	1117	1047	1453	1007	1182	1300	1517	1010	953	1089	793
Cl	ppm	727	770	1383	810	940	767	843	1127	823	813	1167	807	970	793	803	770	1047	1033	690	957
$Fe^{+3}/\sum Fe$		0.282	0.257	0.219	0.247	0.239	0.220	0.233	0.203	0.270	0.241	0.231	0.226	0.232	0.243	0.266	0.240	0.252	0.246	0.247	0.272
Equil. Fo		0.806	0.815	0.725	0.792	0.769	0.780	0.806	0.719	0.806	0.799	0.786	0.753	0.762	0.807	0.793	0.797	0.784	0.789	0.789	0.809
Olivine host																					
SiO_2	wt.%	38.84	39.40	37.75	39.30	38.41	38.33	39.21	38.69	39.62	39.25	38.77	39.24	38.91	39.30	39.79	39.34	39.35	39.23	38.93	39.64
FeO	wt.%	18.28	17.09	24.49	17.19	21.08	18.07	17.95	22.33	17.11	17.73	19.67	20.58	21.37	18.26	17.15	18.81	19.07	19.75	16.93	17.58
TiO_2	wt.%	0.03	0.04	0.04			0.03	0.04			0.02				0.03						
MnO	wt.%	0.34	0.33	0.50	0.33	0.41	0.33	0.36			0.35				0.33					0.29	
MgO	wt.%	42.04	43.88	36.60	42.60	39.49	41.23	42.80	39.77	43.99	43.24	40.92	41.37	40.54	42.69	44.18	42.59	42.38	42.11	42.62	43.23
Cr_2O_3	wt.%	0.01	0.01	0.00			0.01	0.01			0.01				0.00						
NiO	wt.%	0.02	0.07	0.02	0.04	0.02	0.05	0.05	0.01	0.05	0.04	0.03	0.03	0.03	0.03	0.06	0.03	0.03	0.03	0.06	0.05
Total	wt.%	99.57	100.81	99.39	99.45	99.41	98.05	100.42	100.80	100.77	100.64	99.39	101.22	100.84	100.64	101.18	100.77	100.83	101.12	98.83	100.49
Fo		0.804	0.821	0.727	0.815	0.770	0.803	0.810	0.760	0.821	0.813	0.788	0.782	0.772	0.807	0.821	0.801	0.798	0.792	0.818	0.814
Post-entrapment corrected glass																					
Olivine added		0.0%	0.6%	0.1%	2.5%	0.1%	2.3%	0.4%	3.3%	1.6%	1.5%	0.0%	2.6%	0.9%	0.0%	3.1%	0.4%	1.2%	0.3%	2.8%	0.5%
SiO_2	wt.%	46.73	46.64	53.46	46.81	48.40	47.01	47.89	48.09	46.02	46.81	51.51	46.43	47.91	46.49	46.06	45.97	49.55	48.33	47.17	48.32
TiO_2	wt.%	0.77	0.72	0.97	0.64	0.83	0.84	0.77	0.87	0.73	0.76	1.05	0.73	0.80	0.68	0.61	0.66	0.81	0.83	0.82	0.75
Al_2O_3	wt.%	16.79	17.75	16.21	17.25	16.22	18.29	16.45	16.45	17.81	17.66	17.92	17.85	16.83	17.53	17.63	17.21	16.69	16.43	18.27	16.75
FeO*	wt.%	10.30	8.63	9.30	9.72	9.89	9.56	9.86	10.56	9.12	9.24	9.00	10.47	10.40	9.83	9.71	10.70	8.82	9.69	8.62	8.73
FeO	wt.%	7.40	6.43	7.27	7.43	7.53	7.55	7.58	8.57	6.74	7.07	6.92	8.22	8.03	7.44	7.28	8.14	6.66	7.32	6.61	6.38
Fe_2O_3	wt.%	3.23	2.44	2.26	2.55	2.62	2.23	2.53	2.21	2.65	2.40	2.30	2.50	2.63	2.65	2.71	2.84	2.41	2.64	2.23	2.61
MnO	wt.%	0.20	0.20	0.17	0.25	0.27	0.17	0.20	0.22	0.15	0.20	0.17	0.22	0.23	0.18	0.21	0.22	0.17	0.20	0.19	0.17
MgO	wt.%	5.19	4.96	3.26	5.51	4.25	5.18	5.42	4.57	5.20	5.18	4.13	4.96	4.57	5.24	5.61	5.51	4.42	4.68	5.01	4.69
CaO	wt.%	12.30	13.20	8.35	12.47	11.64	12.37	12.19	11.52	12.44	12.24	10.16	12.29	11.17	11.66	13.09	12.02	10.66	11.32	12.73	12.25
Na_2O	wt.%	1.79	1.90	3.31	1.92	2.21	2.26	1.92	2.27	1.74	1.98	2.07	2.06	2.26	2.01	1.67	2.08	2.35	2.31	1.98	2.12
K_2O	wt.%	0.43	0.39	1.36	0.37	0.51	0.53	0.46	0.60	0.36	0.42	0.96	0.47	0.57	0.46	0.37	0.42	0.85	0.66	0.39	0.55
P_2O_5	wt.%	0.13	0.15	0.32	0.11	0.13	0.17	0.15	0.15	0.14	0.12	0.26	0.09	0.14	0.13	0.12	0.14	0.29	0.19	0.11	0.15
Total	wt.%	94.97	94.80	96.93	95.31	94.61	96.59	95.55	95.51	93.98	94.84	96.17	95.81	95.13	94.48	95.35	95.22	94.86	94.90	95.52	94.74
H_2O	wt.%	4.12	2.76	2.12	3.17	4.12	2.66	3.59	2.98	4.49	3.44	2.78	2.92	3.27	3.63	4.12	4.34	4.16	3.93	3.16	3.81
CO_2	ppm	–	–	–	614	–	139	–	–	477	412	–	420	130	457	876	546	395	–	–	–
S	ppm	1474	1118	771	1141	812	1372	777	1016	1552	1100	1045	1417	998	1182	1261	1511	998	950	1060	789
Cl	ppm	727	765	1382	790	939	749	840	1091	810	801	1164	786	961	793	779	767	1034	1030	671	952
$Fe^{+3}/\sum Fe$		0.282	0.254	0.219	0.236	0.238	0.210	0.231	0.188	0.261	0.234	0.230	0.214	0.228	0.243	0.251	0.239	0.245	0.245	0.233	0.269
Mg/[Mg + Fe*]		0.47	0.51	0.38	0.50	0.43	0.49	0.50	0.44	0.50	0.50	0.45	0.46	0.44	0.49	0.51	0.48	0.47	0.46	0.51	0.49

(continued on next page)

Table 1 (*continued*)

Sample		AGR19-02																			
Inclusion #		01	02	03	04	05	07	08	09	10	11	12A[a]	12B	13	14	15	16	17	18	19	20
Mg/[Mg + Fe^{2+}]		0.56	0.58	0.44	0.57	0.50	0.55	0.56	0.49	0.58	0.57	0.52	0.52	0.50	0.56	0.58	0.55	0.54	0.53	0.57	0.57
Olivine–liquid T	°C	1050	1063	1048	1083	1023	1086	1070	1068	1061	1063	1027	1077	1058	1068	1048	1065	1035	1041	1057	1032
log fO_2	1 atm, 1200 °C	−6.50	−6.94	−7.28	−7.07	−7.05	−7.42	−7.13	−7.69	−6.75	−7.09	−7.07	−7.31	−7.12	−6.93	−6.89	−6.99	−6.96	−6.98	−7.15	−6.76
ΔQFM	1 atm, 1200 °C	1.80	1.36	1.02	1.23	1.25	0.88	1.17	0.61	1.55	1.21	1.23	0.99	1.18	1.37	1.41	1.31	1.34	1.32	1.15	1.54
log fO_2	1 kb, ol-liq T	−8.35	−8.60	−9.15	−8.45	−9.18	−8.75	−8.69	−9.28	−8.44	−8.75	−9.25	−8.77	−8.85	−8.51	−8.76	−8.61	−9.03	−8.73	−8.89	−8.88
ΔQFM	1 kb, ol-liq T	1.80	1.37	1.03	1.24	1.25	0.89	1.18	0.62	1.56	1.22	1.23	1.00	1.19	1.38	1.42	1.32	1.34	1.33	1.16	1.54

[a] Inclusion 12A has been corrected for post-entrapment Fe-loss following the method of Danyushevsky et al. (2000).
[b] A "–" indicates data were below detection limit.

al., 1990). Basalt $Fe^{3+}/\sum Fe$ ratio may be translated into oxygen fugacity (fO_2) using the algorithm of Kress and Carmichael (1991), which accounts for the effects of melt composition, pressure, and temperature on the relationship between these two parameters. Referenced at 1200 °C and 1 bar, the Agrigan magma indicates fO_2 conditions from 1.0 to 1.8 log units above the quartz–fayalite–magnetite buffer (QFM; Table 1).

Other geochemical indices are also sensitive to fO_2. In particular, the olivine–liquid partition coefficient for V has been shown to depend strongly on fO_2, due to the differences in incompatibility of the V^{5+}, V^{4+}, and V^{3+} species that make V more incompatible as fO_2 increases (e.g., Canil, 1997, 2002; Canil and Fedortchouk, 2001; Mallmann and O'Neill, 2009). Fig. 1a shows how the concentration of V in olivine vs. melt varies with tectonic setting, comparing olivine–melt inclusion pairs from Agrigan, Marianas and Mt. St. Augustine, Aleutians with olivine-inclusion or glass pairs from the Basin and Range and MORB pillow glass from the East Pacific Rise (see the electronic supplement). The values for $D_V^{ol/liq}$ vary significantly among these four samples, from ~0.01 at Augustine to 0.05 at the mid-ocean ridge. The $Fe^{3+}/\sum Fe$ ratios of these glasses also co-vary with $D_V^{ol/liq}$ (Fig. 1b) along a trajectory most consistent

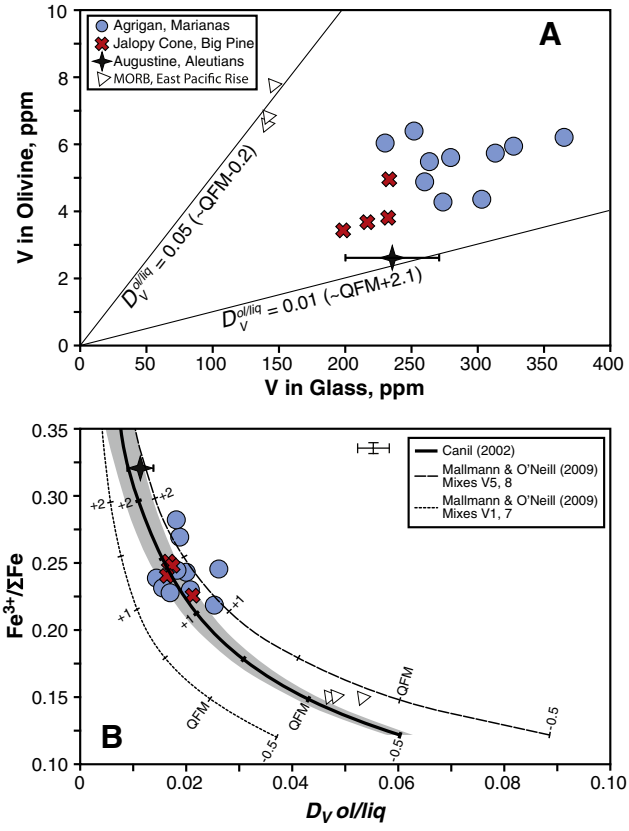

Fig. 1. Vanadium partitioning between olivine and glass as a function of fO_2. (a) Vanadium concentration in glass vs. V concentration in olivine for four global basalts. Lines show constant values of $D_V^{ol/liq}$ that bracket the range observed in the basalts. Each line is labeled with the approximate corresponding fO_2 given by the model of Canil (2002). See the electronic supplement for detailed information on the samples and data shown. (b) $D_V^{ol/liq}$ vs. $Fe^{3+}/\sum Fe$ ratios of natural basalt glasses. Curves shown are modeled using relations between $D_V^{ol/liq}$ and fO_2 reported by Canil (2002) and Mallmann and O'Neill (2009), in combination with the major element composition of inclusion AGR19-02-01, P = 1 atm, T = 1200 °C to translate $Fe^{3+}/\sum Fe$ ratio into fO_2 (in log units relative to the QFM buffer) using the algorithm of Kress and Carmichael (1991). The model curves thus apply exclusively to this one composition, although the curves will be similar for the range of basalt compositions shown. Tick marks for fO_2 are therefore considered approximate, and should be referenced with appropriate caution. Gray shading represents a confidence envelope for the Canil (2002) model curve that accounts for analytical uncertainty in $D_V^{ol/liq}$ (see the electronic supplement). A representative error bar is shown for reference.

with the modeled relationship between $D_V^{ol/liq}$ and fO_2 from Canil (2002), which is derived from mineral/melt partitioning experiments performed using basaltic and komatiitic compositions. More recent partitioning experiments (Mallmann and O'Neill, 2009) define curves of similar functional form, but reveal a significant compositional dependence to $D_V^{ol/liq}$ as a function of fO_2. These experiments, however, are based on unusual, synthetic melt compositions that are unlike most terrestrial basalts, and thus may not provide the optimal reference for natural basalts on Earth. An error analysis accounting for analytical uncertainty in V concentration in glass and olivine reveals that uncertainty in the Canil (2002) model may be as much as ±0.25 log units of fO_2 in the range of QFM + 1 to 1.5, and this uncertainty also increases as fO_2 increases (see the electronic supplement). More importantly, however, the determinations of $D_V^{ol/liq}$ and $Fe^{3+}/\sum Fe$ ratio are not in perfect agreement with any of the three models shown on Fig. 1b. When referenced to the model of Canil (2002), for example, $D_V^{ol/liq}$ values for individual samples disagree with $Fe^{3+}/\sum Fe$ ratios by as much as $Fe^{3+}/\sum Fe = 0.05$ (corresponding to 0.7 log units in fO_2), which we consider the practical uncertainty for using $D_V^{ol/liq}$ as a proxy for fO_2. Moreover, above $Fe^{3+}/\sum Fe$ ~0.25 ($D_V^{ol/liq} < 0.02$), the dynamic range in $D_V^{ol/liq}$ is small relative to the possible variation in $Fe^{3+}/\sum Fe$, such that this method loses resolution for the most oxidized melts. As such, compared to $Fe^{3+}/\sum Fe$ ratio, $D_V^{ol/liq}$ provides a relatively coarse, though useful, index of magmatic redox conditions, and may prove particularly informative at low fO_2 where the uncertainty in $D_V^{ol/liq}$ is smaller and uncertainties in $Fe^{3+}/\sum Fe$ ratio become larger (Cottrell et al., 2009). The broad agreement between $D_V^{ol/liq}$ and $Fe^{3+}/\sum Fe$ ratios of these global basalts further supports the view that the Fe speciation of these melt inclusions did not change on rapid time scales (faster than V could diffusively reequilibrate in olivine) and is therefore a faithful record of magmatic fO_2.

3.3. Degassing and crystallization of the Agrigan Magma

Co-variations of major elements and dissolved volatiles in the Agrigan glass inclusions indicate that the magma experienced synchronous crystallization and degassing prior to eruption. Degassing is assessed by comparing co-variations of dissolved volatiles of differing vapor/melt solubility. The solubility of CO_2, for example, is highly pressure-dependent and its solubility in basaltic melt decreases significantly with decreasing pressure (Dixon et al., 1995). At crustal pressures, CO_2 solubility is much lower than that of H_2O, such that CO_2 will preferentially be removed to the vapor phase until most of the dissolved CO_2 is removed from the degassing melt. Glass inclusions from Agrigan show a trend in H_2O vs. CO_2 consistent with closed-system degassing of a magma with initial H_2O content of ~4.5 wt.% (Fig. 2a). This magmatic H_2O content is lower than has been shown for other Agrigan magmas (up to 5.5 wt.%; Kelley et al., 2010; Shaw et al., 2008), although the maximum CO_2 and H_2O of each magma points to a saturation pressure of ~3 kb, suggesting a common magma storage depth of about 10 km in the crust beneath Agrigan. The melt–fluid partitioning of S in basaltic melt is still poorly constrained experimentally, but depends on P, T, fO_2, fS_2, and melt composition. Empirical co-variations of H_2O and S in arc magmas suggest that melt–fluid partitioning of S may be intermediate between CO_2 and H_2O in mafic arc magmas (Kelley et al., 2010; Sisson and Layne, 1993; Wade et al., 2006) and ranges from 5 to 100, in general agreement with partitioning experiments (Webster and Botcharnikov, 2011). The AGR19-02 magma shows S concentrations broadly decreasing with H_2O, consistent with trajectories shown by other Agrigan magmas, in support of the interpretation that S and H_2O degassed together (Fig. 2b).

Major element concentrations in Agrigan glass inclusions also show evidence of multiphase fractional crystallization of olivine ± clinopyroxene ± plagioclase. The AGR19-02 magma reaches saturation with plagioclase at ~5 wt.% MgO, at which point Al_2O_3 begins to decrease and TiO_2 begins to increase with decreasing MgO (Fig. 3a–b). The point of plag-in for this magma may be slightly earlier than other Agrigan magmas due to its lower H_2O content (Fig. 3a; Kelley et al., 2010; Shaw et al., 2008). At >5 wt.% MgO, the range in data are limited, and are consistent with saturation of either olivine-only or olivine + cpx. A clear change in the redox conditions of the magma is also evident with fractional crystallization (Fig. 3c–f). As MgO of the inclusions decreases, the $Fe^{3+}/\sum Fe$ ratios clearly decrease from a maximum of 0.282 (average 0.25 for all inclusions with >5 wt.% MgO) to a minimum of 0.219 at ~3.2 wt.% MgO. To translate these ratios into oxygen fugacity at magmatic conditions, we assume a mean magmatic pressure of 1 kb, calculate magmatic temperatures using olivine–liquid thermometry (Médard and Grove, 2007; Putirka et al., 2007), and use the algorithm of Kress and Carmichael (1991) to calculate fO_2 in log units relative to the quartz–fayalite–magnetite buffer (ΔQFM) at the magmatic conditions for each inclusion (Table 1). These calculations indicate that magmatic fO_2 conditions decreased from QFM + 1.8 to QFM + 1.0 during the differentiation period preserved by these glass inclusions.

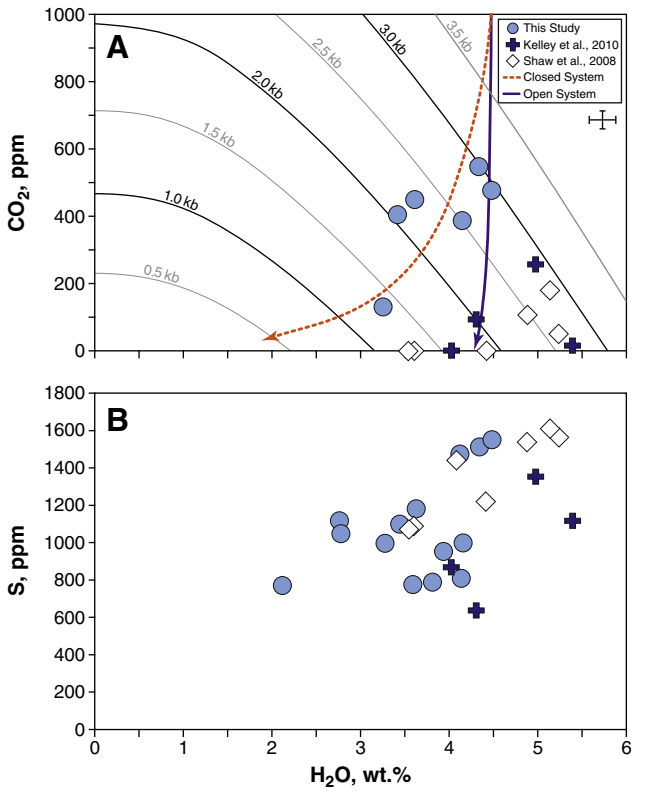

Fig. 2. Dissolved volatile elements in olivine-hosted glass inclusions from Agrigan, Marianas, comparing data from this study (shaded circles) with those of prior work from Shaw et al. (2008; open diamonds) and Kelley et al. (2010; filled crosses). (a) Plot of H_2O vs. CO_2 concentrations. Degassing curves and isobars were calculated at 1100 °C using VolatileCalc (Newman and Lowenstern, 2002). Initial conditions for the open-system degassing curve are 1000 ppm CO_2 and 4.5 wt.% H_2O, and the closed-system curve assumes 2% vapor exsolved. A representative error bar is shown for reference. (b) Plot of H_2O vs. S concentrations. Data show a broad trend towards coincidentally decreasing H_2O and S concentrations during degassing.

4. Discussion

The $Fe^{3+}/\Sigma Fe$ ratios of the Agrigan glass inclusions decrease significantly during the recorded period of differentiation, showing that the magma experienced reduction, not oxidation, by magmatic processes prior to eruption. In the case of this arc magma, the most mafic inclusions are the most oxidized. In the sections that follow,

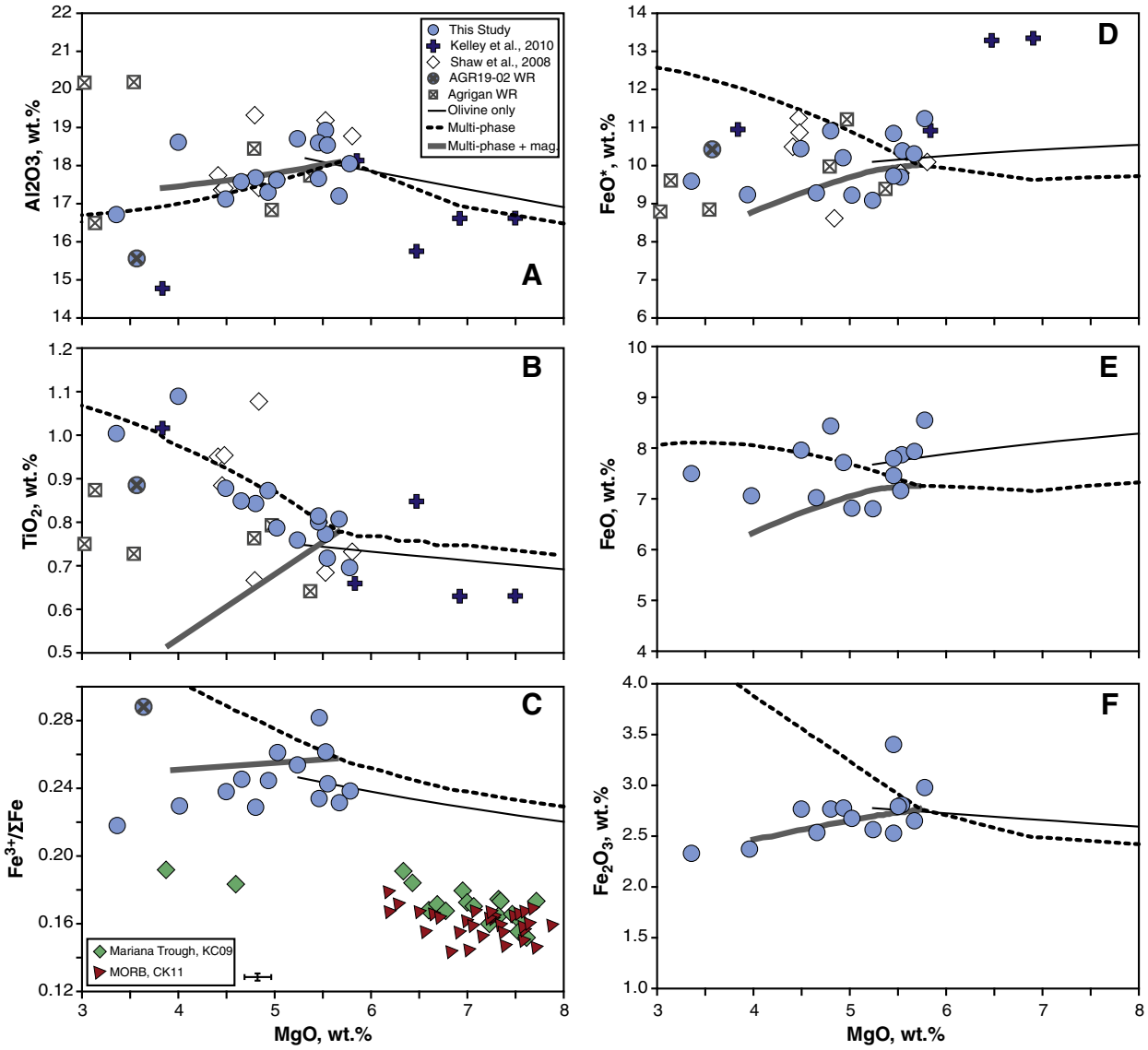

Fig. 3. Major element variations and liquid lines of descent (LLD's) for olivine-hosted glass inclusions from Agrigan, Marianas, comparing data from this study (shaded circles) with those of prior work from Shaw et al. (2008; open diamonds) and Kelley et al. (2010; filled crosses). Also shown are Mariana arc whole-rock data from Elliott et al. (1997; crossed squares), and the whole-rock composition of weathered matrix fragments from the AGR19-02 tephra (crossed circle). Note that the glass inclusions are normalized to anhydrous compositions for comparison with the whole-rock data. Model curves trace trajectories of olivine-only fractional crystallization (thin solid line), multiphase fractionation of ol ± cpx ± plag (dotted line), and multiphase fractionation of ol + cpx + plag + magnetite (thick gray line). Multiphase crystallization was modeled using Petrolog3 (Danyushevsky and Plechov, 2011) at 1 kb, assuming a system closed to oxygen exchange and using the mineral solution models of Ariskin and Barmina (1999) and Danyushevsky (2001). Plots of MgO vs. (a) Al_2O_3, (b) TiO_2, (c) $Fe^{3+}/\sum Fe$ ratio, (d) FeO* (where * indicates total Fe expressed as FeO), (e) FeO (i.e., the true Fe^{2+} concentration expressed as FeO), and (f) Fe_2O_3. Error bars are smaller than the symbol size, except where shown.

we explore several possible explanations for these observations and their consequences for the oxygen fugacity of the Agrigan mantle source.

4.1. Magmatic reduction during differentiation

4.1.1. Magnetite fractionation

Perhaps the most likely potential process for accomplishing magmatic reduction during arc basalt differentiation involves the saturation and fractional crystallization of magnetite (Fe_3O_4) from the magma. Magnetite is a common phase in arc basalts, and is present as a phenocryst phase in sample AGR19-02. Because the Fe in magnetite is mixed valence and dominantly ferric ($2Fe^{3+}$:$1Fe^{2+}$), magnetite fractionation in a system closed to oxygen would decrease both the $Fe^{3+}/\sum Fe$ ratio and the FeO* content of the melt through the preferential removal of this Fe-rich mineral with $Fe^{3+}/\sum Fe = 0.67$. The ability of fractional crystallization to accomplish magmatic reduction in this way, however, requires the magma to be magnetite-saturated over the recorded segment of the liquid line of descent. Fig. 3 shows that, when examined together, FeO*, FeO, Fe_2O_3, and $Fe^{3+}/\sum Fe$ ratios do not decrease with MgO in a manner consistent with models of magnetite fractionation, although there is some scatter to the data. Magnetite fractionation is also expected to strongly decrease the TiO_2 and V concentrations of the melt (e.g., Jenner et al., 2010), which is not observed (Fig. 3b) and calls this potential explanation of the overall reduction trend, starting at 5 wt.% MgO, into question.

In fact, late magnetite crystallization is expected from sample AGR19-02, which is a hydrous magma that straddles the boundary between calc-alkaline and tholeiitic magma series. Fig. 4 shows the ternary AFM discrimination diagram (Irvine and Baragar, 1971), which segregates tholeiitic and calc-alkaline magma series by highlighting the point at which FeO* begins to decrease with

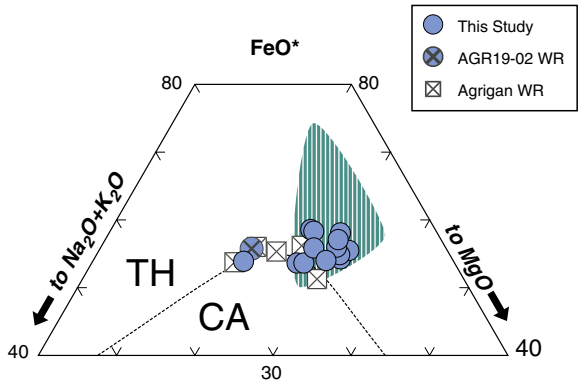

Fig. 4. A cropped ternary plot of total alkalis vs. FeO* vs. MgO (AFM). The dotted line is the discriminating line between tholeiitic (TH) and calc-alkaline (CA) fields from Irvine and Baragar (1971).. Data from Kelley et al. (2010), Kent and Elliott (2002), and Shaw et al. (2008) are encompassed by the striped field for clarity. Note that the Kent and Elliott (2002) data are crystallized inclusions that were re-homogenized at fO_2 = QFM, for which FeO* may have been perturbed by the homogenization process.

decreasing MgO and increasing alkalis during crystallization. Early magnetite crystallization will drive FeO* down in the melt as fractionation progresses, driving basalt compositions into the calc-alkaline field. Late magnetite crystallization, as in the case of AGR19-02, allows basalts to become relatively enriched in FeO*, keeping them in the tholeiitic field above the curved discrimination line (Fig. 4). The evidence for late magnetite saturation in this sample is thus not surprising, given that melt inclusion and whole-rock compositions for Agrigan are mildly tholeiitic according to the definitions of Irvine and Baragar (1971) or Miyashiro (1974). To be clear, however, calc-alkaline and tholeiitic magma series are two end-members along a compositional continuum, and assignment of either of these classifications to a given magma depends in part on the criteria used to classify. For example, Zimmer et al. (2010) assign Agrigan a mildly calc-alkaline affinity using their "Tholeiitic Index," but show that its position near their calc-alkaline/tholeiitic discriminating line is consistent with global arc magmas with dissolved H_2O contents between 2 and 4 wt.%. Moreover, models of LLD's for oxidized (QFM + 1) and variably water-rich (1–6 wt.% H_2O) arc magmas, which are appropriate for the Agrigan composition, predict magnetite saturation at ~4 wt.% MgO (Zimmer et al., 2010), which is approximately where we estimate it based on the melt inclusion compositions. We therefore conclude that magnetite fractionation cannot be responsible for the overall reduction trend recorded by the melt inclusions.

4.1.2. Sulfur degassing

Another, perhaps more likely, candidate for changing magmatic redox conditions without affecting FeO* concentration is magmatic S degassing. The 8 electron difference between oxidized sulfate (S^{6+}) and reduced sulfide (S^{2-}) species dissolved in basaltic melt gives sulfur great potential to drive changes in redox despite its comparatively low abundance. Moreover, when S exsolves from magmas as a vapor phase, its dominant species is SO_2 gas (S^{4+}; Oppenheimer, 2003; Wallace, 2005). The movement of S from its dissolved state in a basaltic melt, where it speciates exclusively as either S^{6+} or S^{2-} (or as mixtures of the two), to a vapor phase of dominantly S^{4+} thus requires electrons in the melt to be redistributed during S degassing (Métrich et al., 2009). Evidence of magmatic reduction accompanied by S degassing has been found at Kilauea volcano (Anderson and Wright, 1972), although SO_2 degassing could drive magmatic fO_2 to either more reduced or more oxidized conditions depending on the initial S speciation of the magma (a function of fO_2) and the relative vapor/melt solubilities of S^{6+} and S^{2-} (Métrich et al., 2009).

The Agrigan data show that decreasing dissolved S concentrations, indicative of S degassing, correlate with decreasing $Fe^{3+}/\sum Fe$ ratios in the glass inclusions (Fig. 5). Moreover, S concentrations in the melt inclusions decrease with MgO, suggesting that coincident crystal fractionation and S degassing took place in this magma. The magma is not sulfide-saturated, as the sulfur content at sulfide saturation at these fO_2s (~0.3–1.3 wt.%; Jugo et al., 2010) is significantly higher than the measured S concentrations of the AGR19-02 melt inclusions (<1600 ppm), and Cu concentrations are too high (90–157 ppm) for a melt in equilibrium with sulfide (Jenner et al., 2010). We constructed a simple degassing model to assess whether enough electrons could be supplied by S to accomplish the magnitude of reduction observed (Fig. 5). The model results suggest that S^{2-} may have lower vapor/melt solubility in this magma than does S^{6+}. Although few quantitative constraints currently exist for vapor/melt partitioning of different S species, this relative sense of solubility is consistent with the known solubilities of S species in silicate melts. At high fO_2, S solubility in basalt increases significantly because S^{6+} is more soluble (Carroll and Rutherford, 1988; Jugo et al., 2010; Wallace and Carmichael, 1994). In this highly simplified case, we find that enough electrons could be supplied by the conversion of dissolved S^{2-} to SO_2 gas to accommodate the observed change in Fe speciation (Fig. 5). It is important to note, however, that this model represents an oversimplification of natural systems, where Fe, S, and other redox-sensitive elements will all respond to the changing electronic balance in the melt, so this example explores an end-member case. Though the model is speculative by necessity, due to the paucity of quantitative constraints on the vapor/melt partitioning of S species, the trend shown by the data evokes a link between S degassing and Fe redox in this magma.

4.2. Alternative hypotheses for differentiation-related oxidation mechanisms

Of course, there is a chance that oxidation does happen during differentiation, but our sampling of the Agrigan magma has failed to capture the oxidizing segment of the LLD. Here we explore some outstanding hypotheses for processes by which magmas could

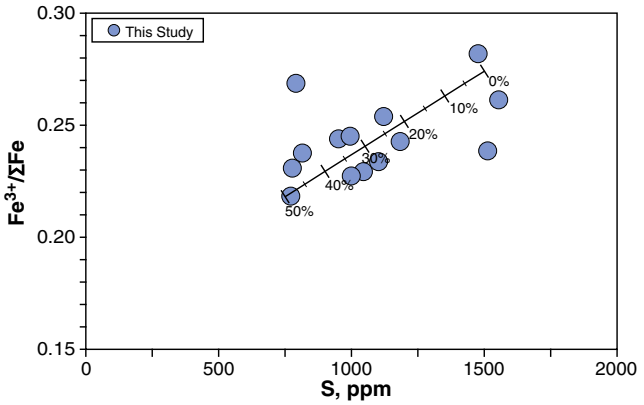

Fig. 5. Plot of S vs. $Fe^{3+}/\sum Fe$ ratio in olivine-hosted glass inclusions from Agrigan, Marianas, showing the redox change correlated with S degassing. The thin line with tick marks is the S degassing model discussed in Section 4.1.2. Tick marks identify percentages of S degassed from the magma. The model starts with initial conditions of the magma at 9.64 wt.% FeO*, 1500 ppm S, $Fe^{3+}/\sum Fe = 0.28$, and $S^{6+}/\sum S = 0.83$ (S-speciation calculated from fO_2 using Wallace and Carmichael (1994)). Sulfur is assumed to enter the vapor in a $S^{6+}/\sum S$ ratio of 0.35, and all S entering the vapor was assumed to convert to SO_2 (S^{4+}) which assumes different vapor/melt solubilities for S^{2-} and S^{6+}. Electrons left in the melt at each degassing step were completely reassigned to Fe to accomplish reduction of the $Fe^{3+}/\sum Fe$ ratio.

become oxidized during differentiation, and how these relate specifically to the case of the Agrigan magma.

4.2.1. Crystallization of Fe^{2+}-rich phases

Cottrell and Kelley (2011) showed that fractional crystallization of ferromagnesian minerals causes slight oxidation of MORBs during differentiation. Co-crystallization of Fe-poor plagioclase and Fe^{2+}-rich olivine and clinopyroxene slightly increase the melt $Fe^{3+}/\sum Fe$ ratio, and crystallization of Fe^{3+}-rich magnetite (Fe_3O_4) will drive liquid $Fe^{3+}/\sum Fe$ ratios down (Fig. 3c), although crystallization of any realistic combination of these phases is insufficient to create the observed arc compositions from a primary magma of $Fe^{3+}/\sum Fe = 0.14$, appropriate for MORB (Cottrell and Kelley, 2011). Low overall TiO_2 concentrations of arc basalts could be interpreted as evidence that ilmenite ($FeTiO_3$) crystallization may have increased the arc $Fe^{3+}/\sum Fe$ ratios. Ilmenite, however, is not observed in our samples and is an extremely rare phase in arc basalts. Arc basalts commonly have low TiO_2 concentrations due to high extents of H_2O-fluxed mantle melting (Kelley et al., 2006, 2010), withholding of Ti by residual rutile in the slab (Pearce and Parkinson, 1993), and/or more depleted mantle sources beneath arcs relative to spreading ridges (Pearce and Stern, 2006). When present, ilmenite saturates after titanomagnetite, has a significant hematite (Fe_2O_3) component (15–30%; Gill, 1981), and would draw melt TiO_2 concentrations down with progressive crystallization, which is the opposite of our observations (Fig. 3b).

4.2.2. Degassing of H–C–O–Cl species

Co-variations between volatile species, major and trace elements, and magmatic oxidation state implicate S degassing as a potential driving force behind the observed magmatic reduction. It is worth considering, however, the possible effects of degassing other volatile species. Water and CO_2 were degassing from this Agrigan magma during inclusion entrapment (Fig. 2); however, we see no evidence for concomitant oxidation, nor do we expect any. Magmatic "auto-oxidation" during H_2 degassing (Holloway, 2004) can only drive oxidation if initial magmatic conditions are sufficiently reducing (fO_2 < QFM-1) to allow a significant amount of H_2O to dissociate to H_2 in the vapor phase *and* if that vapor phase exits the system out of equilibrium with the magma it is oxidizing (Cottrell and Kelley, 2011; Crabtree and Lange, 2011). This process, which becomes increasingly inefficient and self-limiting as fO_2 increases above QFM, cannot drive magmas to the higher fO_2s observed here (Candela, 1986; Carmichael, 1991; Cottrell and Kelley, 2011; Crabtree and Lange, 2011; Frost and Ballhaus, 1998). Similarly, at fO_2 greater than QFM-1, graphite is not stable and carbon is speciated in the melt as carbonate. Under these conditions, CO_2 vapor loss is fO_2 neutral and cannot drive magmatic fO_2s to the values we observe (Ballhaus, 1993; Cottrell and Kelley, 2011). Chlorine degassing may also drive magmatic oxidation (Bell and Simon, 2011), but there is no evidence for Cl degassing in this eruption. We again conclude that sulfur is the only degassing species for which we see, or expect, a concomitant change in magmatic redox, and in this case the shift is toward reduction.

4.2.3. Oxidation of melt inclusions via outward H^+ diffusion

If H_2O is lost from a melt inclusion after entrapment, the main mechanism by which this takes places is proton (H^+) diffusion through the host olivine. This scenario requires a gradient in H_2O between the inclusion and the external melt and, if the melt inclusion were truly a closed system for fO_2, such a process would result in a simultaneous increase of the inclusion fO_2 due to the buildup of excess oxygen left behind by H_2O dissociation and loss of H^+. Recent experimental work, however, has shown that olivine-hosted melt inclusions are open to fO_2 exchange with the external melt, and that H_2O and fO_2 re-equilibration through olivine take place independently, but at roughly similar rates (e.g., Bucholz et al., 2011; Gaetani et al., 2010). In light of these results, H^+ diffusion cannot drive oxidation of melt inclusions because any resultant change in the inclusion fO_2 will be reset by the host magma at the same rate. At equilibrium, the oxidation state of Fe in inclusions is determined by the oxidation state imposed by the system, be that the host magma, or the environment of a laboratory experiment. The observation of a range of inclusion fO_2s and H_2O contents among the AGR19-02 suite suggests that the pace of re-equilibration of either H_2O or fO_2 in the inclusions must have been slower than the rate at which changes in the external melt occurred, otherwise the inclusions would all have homogeneous H_2O and fO_2. We cannot rule out the possibility that diffusive processes have had minor effects on the inclusion compositions, and emphasize that the measured H_2O concentrations and $Fe^{3+}/\sum Fe$ ratios in the inclusions are thus robust minima. Most importantly, the melt inclusions record a trend of Fe reduction coincident with decreasing H_2O in this suite, which is the opposite of the predicted relationship for H^+-loss in a system closed to oxygen exchange.

4.3. Oxygen fugacity of the Agrigan mantle source

4.3.1. Reconstruction of primary melts

To assess the redox conditions of the mantle source beneath Agrigan, we reconstruct primary mantle melt compositions for the most mafic inclusions (MgO > 5.0 wt.%; n = 6) of the Agrigan suite by calculating the equilibrium olivine for each melt inclusion, and then adding 0.01% of that olivine to each melt composition, and repeating these steps until equilibrium with mantle olivine for a range of possible Fo contents is achieved (Fo_{90}, $Fo_{91.5}$, and Fo_{93}; Table 2; Kelley et al., 2006, 2010; Stolper and Newman, 1994). These most mafic melts are sufficiently close to the modeled point of cpx—in that an assumption of olivine-only on the liquidus results in relatively small error in the reconstructed melts, which require ~18–25% olivine added back to reach Fo_{90} equilibrium. For these calculations, we assumed that the magma evolved in a system closed to oxygen (as is the case for MORBs; Cottrell and Kelley, 2011), so the number of moles of Fe^{3+} in the system remained unchanged as Fe^{2+} from olivine was added back to each melt. The $Fe^{3+}/\sum Fe$ ratios of the Agrigan primary melts are thus lower (0.18–0.22 at Fo_{90}; Table 2) relative to the fractionated starting compositions (0.23–0.28). The dissolved H_2O of these most mafic inclusions is higher on average than the more differentiated inclusions, and we thus assume these are robust minima for the undegassed H_2O content of the magma.

For comparison with the arc, Fig. 6 shows similar reconstructions of MORB (Cottrell and Kelley, 2011) and back-arc basin pillow basalts (BABB) from the Mariana trough (Kelley and Cottrell, 2009). The modeled melt compositions clearly show a progressive increase in the $Fe^{3+}/\sum Fe$ ratios of primary melts that is coincident with increases in geochemical tracers of subduction influence (e.g., dissolved H_2O, Ba/La; Fig. 6a, c), similar to the trends observed for global arc basalts uncorrected for fractionation effects (Fig. 6a inset; Kelley and Cottrell, 2009). Because composition, pressure, and temperature of magmas all influence the direct translation of magmatic $Fe^{3+}/\sum Fe$ ratios into oxygen fugacity (Kress and Carmichael, 1991), fundamental differences in primary melt composition or P–T conditions of origin that vary with tectonic setting could potentially offset the relationship between fO_2 and $Fe^{3+}/\sum Fe$ ratios of magmas. We assess the extent to which these factors could affect interpretations of the data by combining constraints on the pressures and temperatures of last equilibration of primary melts with the mantle (Table 2; Lee et al., 2009) with the primary melt compositions to determine fO_2 for each reconstructed primary melt at relevant P–T conditions in the mantle. Fig. 6b shows that the modeled fO_2s of the mantle sources indicate the same sense of increase from MORB to BABB to Agrigan as do $Fe^{3+}/\sum Fe$ ratios. The Agrigan source is modeled at fO_2 conditions in the range of ΔQFM + 1 to + 1.6 (for a Fo_{90} source; + 0.8 to + 1.3 for the most refractory case), significantly more oxidized than the back-arc basin

Table 2
Reconstructed primary melt compositions from Agrigan, Marianas.

Sample		AGR19-02																	
Inclusion #		01	08	10	11	14	16	01	08	10	11	14	16	01	08	10	11	14	16
Target Fo content		Fo_{90}						$Fo_{91.5}$						Fo_{93}					
Olivine added		22%	22%	18%	20%	22%	25%	32%	32%	26%	29%	32%	36%	46%	46%	39%	42%	46%	52%
SiO_2	wt.%	45.56	46.51	45.16	45.72	45.36	44.81	45.21	46.09	44.88	45.39	45.02	44.50	44.83	45.63	44.54	45.01	44.66	44.16
TiO_2	wt.%	0.63	0.63	0.62	0.63	0.55	0.53	0.59	0.58	0.58	0.59	0.51	0.49	0.53	0.53	0.52	0.53	0.46	0.44
Al_2O_3	wt.%	13.75	13.47	15.12	14.72	14.36	13.73	12.72	12.46	14.13	13.69	13.28	12.66	11.50	11.27	12.81	12.44	12.01	11.33
FeO	wt.%	8.42	8.55	7.63	8.04	8.45	9.17	8.51	8.63	7.76	8.15	8.54	9.21	8.43	8.54	7.75	8.11	8.45	9.04
Fe_2O_3	wt.%	2.65	2.08	2.25	2.00	2.17	2.26	2.45	1.92	2.10	1.86	2.01	2.09	2.21	1.74	1.91	1.69	1.82	1.87
MnO	wt.%	0.17	0.16	0.12	0.17	0.15	0.18	0.15	0.15	0.12	0.16	0.14	0.16	0.14	0.13	0.10	0.14	0.12	0.15
MgO	wt.%	12.70	12.90	11.52	12.12	12.75	13.82	15.46	15.65	13.98	14.72	15.51	16.60	18.87	19.05	17.45	18.05	18.92	20.23
CaO	wt.%	10.07	9.98	10.56	10.20	9.55	9.59	9.32	9.23	9.88	9.48	8.84	8.84	8.42	8.35	8.95	8.62	7.99	7.91
Na_2O	wt.%	1.47	1.57	1.48	1.65	1.64	1.66	1.36	1.45	1.38	1.53	1.52	1.53	1.23	1.32	1.25	1.39	1.37	1.37
K_2O	wt.%	0.35	0.38	0.31	0.35	0.38	0.33	0.33	0.35	0.29	0.33	0.35	0.31	0.30	0.31	0.26	0.30	0.32	0.27
P_2O_5	wt.%	0.11	0.12	0.12	0.10	0.11	0.11	0.10	0.11	0.11	0.09	0.10	0.10	0.09	0.10	0.10	0.08	0.09	0.09
H_2O	wt.%	3.38	2.94	3.81	2.87	2.97	3.46	3.12	2.72	3.56	2.67	2.75	3.19	2.83	2.46	3.23	2.42	2.48	2.86
$Fe^{+3}/\sum Fe$		0.220	0.179	0.210	0.183	0.188	0.182	0.205	0.167	0.196	0.171	0.175	0.169	0.191	0.155	0.181	0.158	0.162	0.157
Temp.	°C	1299	1308	1285	1296	1310	1329	1368	1377	1325	1362	1380	1400	1458	1468	1412	1450	1472	1499
Pressure	GPa	1.52	1.46	1.37	1.45	1.58	1.86	2.01	1.95	1.78	1.90	2.08	2.42	2.81	2.75	2.48	2.65	2.91	3.40
At 1200 °C and 1 atm																			
log fO_2		−7.06	−7.66	−7.24	−7.61	−7.48	−6.34	−7.21	−7.80	−7.38	−7.75	−7.63	−7.70	−7.36	−7.95	−7.54	−7.90	−7.79	−7.86
ΔQFM		1.25	0.65	1.07	0.69	0.82	0.76	1.10	0.50	0.92	0.55	0.67	0.60	0.94	0.35	0.76	0.40	0.51	0.44
At T and P																			
log fO_2		−4.58	−5.15	−5.03	−5.22	−4.86	−4.55	−3.74	−4.29	−4.46	−4.42	−4.01	−3.68	−2.64	−3.19	−3.38	−3.34	−2.90	−2.50
ΔQFM		1.58	0.97	1.38	1.02	1.16	1.11	1.47	0.87	1.28	0.92	1.05	1.00	1.34	0.75	1.16	0.80	0.91	0.81

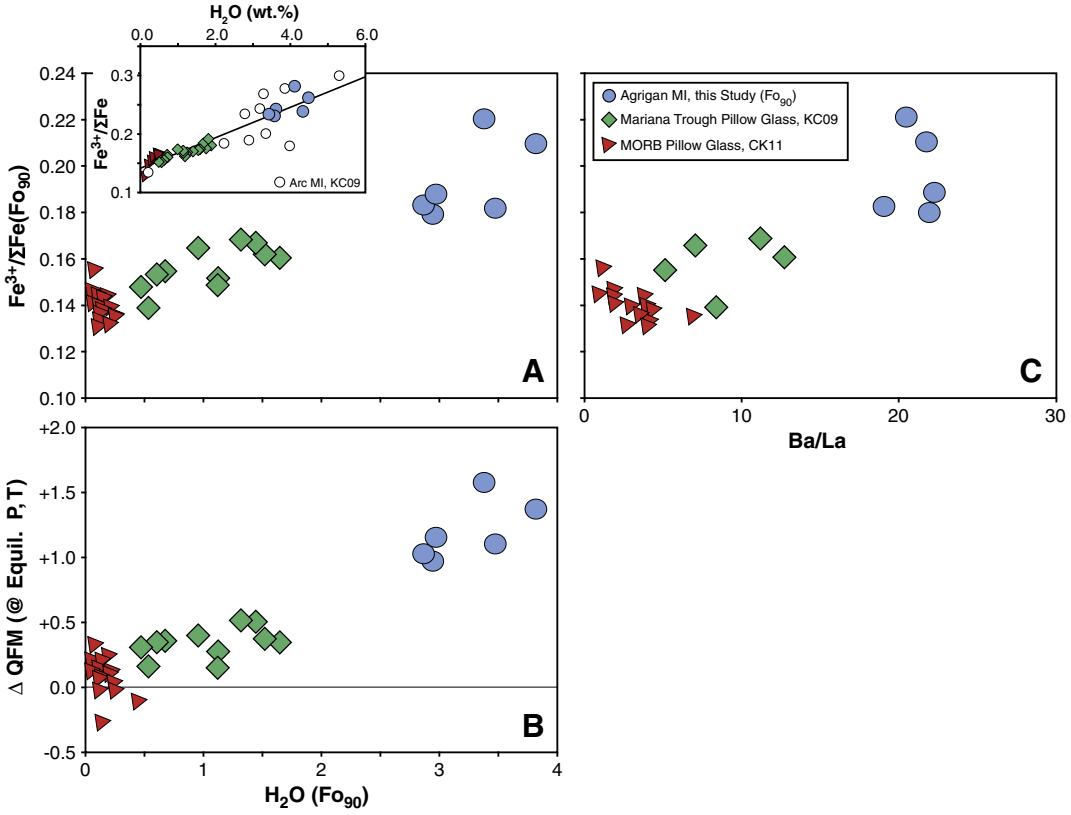

Fig. 6. Modeled primary melt compositions and oxygen fugacities for Agrigan, Marianas. (a) Plot of H_2O vs. $Fe^{3+}/\sum Fe$ ratio in reconstructed primary melts in equilibrium with Fo_{90} olivine. Agrigan data from this study are shaded circles, filtered for the most mafic glass inclusions (MgO > 5 wt.%; see Section 4.3.1). Modeled MORBs (shaded triangles) and Mariana trough basalts (shaded diamonds) are from Cottrell and Kelley (2011) and Kelley and Cottrell (2009). Inset shows H_2O vs. $Fe^{3+}/\sum Fe$ ratios for raw basalt compositions, uncorrected except for PEC, with the addition of global arc data from Kelley and Cottrell (2009; open circles). (b) Plot of H_2O vs. oxygen fugacity (ΔQFM) for reconstructed primary melts in equilibrium with Fo_{90} olivine (Table 2). Oxygen fugacity is referenced to the QFM buffer at the P–T conditions of last equilibration of each melt with the mantle, modeled using melt thermobarometry (Lee et al., 2009). (c) Ba/La ratio vs. $Fe^{3+}/\sum Fe$ ratio for reconstructed primary melts in equilibrium with Fo_{90} olivine.

(ΔQFM +0.2 to +0.5) or MORB (ΔQFM −0.25 to +0.4) sources, and fO_2 increases coincident with increasing primary melt H_2O content and tracers of additions from the subducted slab to the mantle source. Compositional differences among the modeled primary melt compositions should no longer reflect variations driven by differentiation processes. Melt inclusions are well-known to preserve compositional diversity that reflects true heterogeneity of primary melts that aggregated to form larger magma bodies (e.g., Saal et al., 1998; Sobolev and Shimizu, 1993), and the weak correlation of reconstructed Agrigan primary melt compositions in Fig. 6 may thus reflect diversity in discrete primary melts at Agrigan. We emphasize that the H_2O content of arc magmas is a useful tracer of the influence of subduction on the arc mantle source, but H_2O itself is unlikely to be the ultimate cause of oxidation (e.g., Frost and Ballhaus, 1998; Kelley and Cottrell, 2009). Although the oxidation state and water content of olivine-hosted melt inclusions may be reset by the diffusion of H^+ and point defects in the presence of chemical gradients (e.g., Bucholz et al., 2011; Gaetani et al., 2010), this would eliminate, or at least diffuse, the strong correlations we observe between oxidation state and major, trace, and volatile elements. The data arrays seen in Fig. 6, for example, are not consistent with concomitant loss of H from and oxidation of the Agrigan inclusions.

4.3.2. Trace element proxies for source fO_2

The Agrigan data set offers an opportunity to directly compare multiple proxies for the oxidation state of the arc mantle source. The oxidation state of iron in the most mafic inclusions indicates derivation from a mantle source 1–1.5 orders of magnitude more oxidized than the MORB mantle source (Fig. 6; Cottrell and Kelley, 2011) and we have identified no process during the subsequent evolution of this magma in the crust to oxidize Fe. Two trace element proxies for source fO_2 provide an independent assessment of our analysis: the V/Sc ratio (Canil, 1997; Lee et al., 2003, 2005) and the Zn/Fe ratio (Lee et al., 2010).

The V/Sc ratios of the least-evolved Agrigan inclusions provide a maximum constraint on V/Sc of primitive Agrigan magmas (and by proxy on fO_2) because clinopyroxene fractionation increases V/Sc ratios in the melt. These lowest Agrigan ratios overlap the MORB field and fall between 6 and 8. For these inclusions, representing 15–20% melt fraction (Kelley et al., 2010), the modeled fO_2 falls between ~QFM and QFM-1 (see the electronic supplement). This completely overlaps the MORB source, consistent with Lee et al. (2005), and is in opposition to the fugacities calculated from Fe speciation. The discrepancy between the Fe and V/Sc proxies is surprising in this case because our detailed study of this eruptive suite indicates that neither crystallization nor degassing, the two processes most often invoked to explain this discrepancy, are primarily responsible for oxidation of this magma since it last equilibrated with the mantle source. The reason for this discrepancy remains unknown, but it is possible that the calibration conditions for the V/Sc proxy are inappropriate for melting in the hydrous mantle wedge (Jackson et al., 2010).

The Zn/Fe ratios in the Agrigan glass inclusions broadly increase as differentiation proceeds (see the electronic supplement) with the most mafic inclusions bearing ratios of 7–12. Clinopyroxene and magnetite fractionation can only drive the Zn/Fe ratio up, therefore the lowest Zn/Fe ratio we observe in this suite (7.6) provides a minimum fO_2 for this system's mantle source of QFM + 2 (Lee et al., 2010), consistent with the Lee et al. (2010) compilation for Mariana

whole rock data and the oxidation state of Fe determined in this study.

4.4. An oxidized arc mantle wedge

4.4.1. Ferric Fe content of the arc mantle

Reconstructed primary melts for Agrigan may be inverted for mantle melt fraction, using TiO_2 as a proxy for melt fraction and a simple batch melting model, with constraints from Kelley et al. (2010). The batch melting equation may then be re-arranged to solve for the equivalent concentrations of H_2O and Fe^{3+} of the Agrigan mantle source, using appropriate mantle/melt partition coefficients for H_2O (0.008; average of Aubaud et al., 2004, and Hauri et al., 2006), and Fe_2O_3 (0.1–0.2; Canil et al., 1994; Mallmann and O'Neill, 2009). These calculations indicate that the arc mantle relevant for Agrigan basalts contains 0.49–0.87 wt.% Fe_2O_3 and 0.48–0.72 wt.% H_2O. This Fe_2O_3 content is bracketed by the Fe_2O_3 concentration predicted for the background MORB mantle source (≥0.3 wt.%; Cottrell and Kelley, 2011) and the range predicted for oxidized, hydrated arc mantle based on similar modeling of Fe_2O_3 in whole-rock arc lavas (0.6–1.0 wt.%; Parkinson and Arculus, 1999). Subtracting the Fe_2O_3 contribution from the background mantle (0.3 wt.%) yields excess concentrations of 0.19–0.57 wt.% Fe_2O_3 added to (or created in) the arc mantle by slab-derived components, and maximum Fe_2O_3/H_2O ratios for the slab-derived components of 0.4–1.0 on a weight basis (0.04–0.11 Fe_2O_3/H_2O or 0.09–0.23 Fe^{3+}/H_2O on a molar basis). Such a high proportion of Fe_2O_3 to H_2O cannot be added directly by a dilute, oxidized aqueous fluid because Fe^{3+} has low solubility in such fluids (Schneider and Eggler, 1986). As slab-derived components become more solute-rich, however, Fe^{3+} is likely to become much more mobile, as has been shown for other fluid-immobile elements (e.g., Johnson and Plank, 1999; Kessel et al., 2005). Therefore, if all of the observed excess Fe^{3+} is transported directly from the slab into the mantle wedge, these constraints require that slab-derived, H_2O-rich components are hypersaline brines, supercritical fluids, or silicate melts of subducted sediments or the basaltic plate.

Alternatively, fluid-mobile elements, such as S, could oxidize the mantle wedge of subduction zones without requiring direct transport of Fe^{3+}. If the intrinsic oxygen fugacity of fluids released from the descending slab are sufficiently high to carry S as sulfate (SO_4^{2-}; S^{6+}), then 1 mol of S has the potential to oxidize 8 mol of Fe^{2+} as sulfate in the fluid is reduced to form sulfide (S^{2-}) in the mantle wedge. Sulfur reduction will take place provided that the oxygen fugacity of the mantle wedge remains below the sulfur–sulfur oxide (SSO) buffer, or approximately QFM + 2 (Mungall, 2002). The molar S/H_2O ratio required to oxidize 0.09–0.23 mol of Fe^{3+} per mole of H_2O is 0.011–0.028. Constraints on the S content of various mantle sources suggest that arc mantle contains ~200 ppm S in excess of MORB mantle (Wallace, 2005), and given the above constraints on the H_2O content of the Agrigan mantle source, this gives a molar S/H_2O ratio in slab-derived components of ~0.016–0.023. From this perspective, hydrous slab-derived components could deliver enough S to create the observed Fe^{3+} abundance in the arc mantle.

4.4.2. Potential sources and causes of oxidation in the mantle wedge

Subducting oceanic lithosphere is highly oxidized (e.g., Alt et al., 1986; Berndt et al., 1996; Lecuyer and Ricard, 1999). Sediments may contain $Fe^{3+}/\sum Fe$ ratios up to 0.82 and altered basalts up to 0.19–0.24 (Lecuyer and Ricard, 1999). The lithospheric mantle may also become oxidized through the formation of serpentine and brucite, which exclude Fe from their olivine protolith that then forms magnetite (and H^+, which escapes the system) at the expense of H_2O (e.g., Berndt et al., 1996). The above discussion (Section 4.4.1) proposes that this oxidized subducted plate provides the materials, potentially in the form of Fe^{3+} or SO_4^{2-}, that drive oxidation of the mantle wedge beneath arc volcanoes. Sulfur isotopic studies of Mariana fore-arc serpentinites and arc lavas suggest that S is delivered by the slab, and specifically by the subducted sediment, to the mantle wedge (Alt and Shanks, 2006; Alt et al., 1993), although S abundances and budgets of subducting sediments in the Marianas and elsewhere remain poorly constrained (Plank and Langmuir, 1998). Serpentinized lithospheric mantle also has the potential to produce highly oxidized fluids during de-serpetinization reactions that consume magnetite during dehydration (Elburg and Kamenetsky, 2007; Nozaka, 2003).

Oxidized slab-derived fluids, however, have no power to change the mantle wedge fO_2 if the mantle is buffered by mineral equilibria, which, through changes in mineral mode, may mediate system fO_2. Recent work postulated that the relatively dry and reduced MORB source may be buffered during melting near QFM by S equilibria (Cottrell and Kelley, 2011). The buffering capacity of the arc source, however, may be diminished by the presence of H_2O which, through increased melt fraction, may deplete the mantle wedge of buffering phases. This could leave arc melts more susceptible to oxidation by the addition of oxidized fluids (Evans and Tomkins, 2011).

5. Conclusions

Olivine-hosted glass inclusions from Agrigan, Marianas preserve a segment of the liquid line of descent of a H_2O-rich arc magma. Glass compositions are uniformly more oxidized than MORBs, and indicate reduction, rather than oxidation, as the major redox change during differentiation. Correlation between $Fe^{3+}/\sum Fe$ ratios and dissolved S concentrations indicate that S degassing may play a major role in modifying melt redox during degassing. Reconstruction of the most mafic Agrigan melts to primary mantle melt compositions, which compensates for the slight oxidation effect of fractionating Fe^{2+}-rich crystal phases, shows that primary arc melts are oxidized at equilibrium with the arc mantle source, and that fO_2 correlates directly with indices of slab additions to the mantle wedge (e.g., H_2O, Ba/La). Simple mass balance calculations suggest that S derived from the subducted plate is present in the arc wedge in sufficient abundance to accommodate the magnitude of oxidation required.

Acknowledgments

We are grateful for thorough reviews from Cin-Ty Lee, Chris Ballhaus, and Leonid Danyushevsky. We acknowledge constructive discussions with and inspiration from Cin-Ty Lee, Marc Hirschmann, Mac Rutherford, and Becky Lange. Terry Plank generously shared the source sample material and unpublished data to assist with this study, in addition to valuable thoughts and data on V partitioning. This work was made possible by the contributions of Benjamin Parks, who generated a pilot data set for this study through the GSO SURFO program, and Maryjo Brounce and Christa Jackson, who assisted in all aspects of data collection. Tony Lanzirotti contributed invaluable expertise in μ-XANES analysis and beamline operations at X26A. NSF Award OCE-0644625 provided curatorial support for marine geological samples at the University of Rhode Island. Use of the National Synchrotron Light Source, Brookhaven National Laboratory, was supported by the U.S. Department of Energy, Office of Science, Office of Basic Energy Sciences, under Contract No. DE-AC02-98CH10886. We acknowledge support from Smithsonian's Scholarly Studies Program (EC), a URI ADVANCE fellowship (KK) and NSF awards EAR-0838328 (KK), MARGINS-EAR-0841108 (KK) and MARGINS-EAR-0841006 (EC).

Appendix A. Supplementary data

Supplementary data to this article can be found online at doi:10.1016/j.epsl.2012.02.010.

References

Alt, J., Shanks, W., 2006. Stable isotope compositions of serpentinite seamounts in the Mariana forearc: serpentinization processes, fluid sources and sulfur metasomatism. Earth Planet. Sci. Lett. 242, 272–285. doi:10.1016/j.epsl.2005.11.063.

Alt, J.C., Honnorez, J., Laverne, C., Emmermann, R., 1986. Hydrothermal alteration of a 1 km section through the upper oceanic crust, Deep Sea Drilling Project Hole 504B: Mineralogy, chemistry, and evolution of seawater–basalt interactions. J. Geophys. Res. 91, 10309–10355.

Alt, J.C., Shanks III, W.C., Jackson, M.C., 1993. Cycling of sulfur in subduction zones: the geochemistry of sulfur in the Mariana Island Arc and back-arc trough. Earth Planet. Sci. Lett. 119, 477–494.

Anderson, A.T., Wright, T.L., 1972. Phenocrysts and glass inclusions and their bearing on oxidation and mixing of basaltic magmas, Kilauea volcano, Hawaii. Am. Mineral. 57, 188–216.

Ariskin, A.A., Barmina, G.S., 1999. An empirical model for the calculation of spinel–melt equilibria in mafic igneous systems at atmospheric pressure: 2. Fe–Ti oxides. Contrib. Mineral. Petrol. 134, 251–263. doi:10.1007/s004100050482.

Aubaud, C., Hauri, E.H., Hirschmann, M.M., 2004. Hydrogen partition coefficients between nominally anhydrous minerals and basaltic melts. Geophys. Res. Lett. 31. doi:10.1029/2004GL021341.

Ballhaus, C., 1993. Redox states of lithospheric and asthenospheric upper mantle Contrib. Mineral. Petrol. 114, 331–348.

Bell, A.S., Simon, A., 2011. Experimental evidence for the alteration of the Fe3+/Fe of silicate melt caused by the degassing of chlorine-bearing aqueous volatiles. Geology 39, 499–502. doi:10.1130/g31828.1.

Berndt, M.E., Allen, D.E., Seyfried, W.E., 1996. Reduction of CO2 during serpentinization of olivine at 300 °C and 500 bar. Geology 24, 351–354.

Brandon, A.D., Draper, D.S., 1996. Constraints on the origin of the oxidation state of mantle overlying subduction zones: an example from Simcoe, Washington, USA. Geochim. Cosmochim. Acta 60, 1739–1749.

Bucholz, C.E., Gaetani, G.A., Behn, M.D., 2011. Diffusive re-equilibration of volatiles and oxygen fugacity in olivine-hosted melt inclusions: experiments and numerical models. EOS Transactions AGU, V11H-02.

Candela, P.A., 1986. The evolution of aqueous vapor from silicate melts: effect on oxygen fugacity. Geochim. Cosmochim. Acta 50, 1205–1211.

Canil, D., 1997. Vanadium partitioning and the oxidation state of Archaean komatiite magmas. Nature 389, 842–845.

Canil, D., 2002. Vanadium in peridotites, mantle redox and tectonic environments: Archean to present. Earth Planet. Sci. Lett. 195, 75–90.

Canil, D., Fedortchouk, Y., 2001. Olivine–liquid partitioning of vanadium and other trace elements, with applications to modern and ancient picrites. Can. Mineral. 39, 319–330. doi:10.2113/gscanmin.39.2.319.

Canil, D., O'Neill, H.S.C., Pearson, D.G., Rudnick, R.L., McDonough, W.F., Carswell, D.A., 1994. Ferric iron in peridotites and mantle oxidation states. Earth Planet. Sci. Lett. 123, 205–220.

Carmichael, I.S.E., 1991. The redox states of basic and silicic magmas: a reflection of their source regions? Contrib. Mineral. Petrol. 106, 129–141. doi:10.1007/BF00306429.

Carroll, M.R., Rutherford, M.J., 1988. Sulfur speciation in hydrous experimental glasses of varying oxidation state: results from measured wavelength shifts of sulfur X-rays. Am. Mineral. 73, 845–894.

Christie, D.M., Carmichael, I.S.E., Langmuir, C.H., 1986. Oxidation states of mid-ocean ridge basalt glasses. Earth Planet. Sci. Lett. 79, 397–411.

Cottrell, E., Kelley, K.A., 2011. The oxidation state of Fe in MORB glasses and the oxygen fugacity of the upper mantle. Earth Planet. Sci. Lett. 305, 270–282. doi:10.1016/j.epsl.2011.03.014.

Cottrell, E., Kelley, K.A., Lanzirotti, A.T., Fischer, R.A., 2009. High-precision determination of iron oxidation state in silicate glasses using XANES. Chem. Geol. 268, 167–179. doi:10.1016/j.chemgeo.2009.08.008.

Crabtree, S.M., Lange, R.A., 2011. An evaluation of the effect of degassing on the oxidation state of hydrous andesite and dacite magmas: a comparison of pre- and post-eruptive Fe2+ concentrations. Contrib. Mineral. Petrol.. doi:10.1007/s00410-011-0667-7

Danyushevsky, L.V., 2001. The effect of small amounts of H_2O on crystallization of mid-ocean ridge and backarc basin magmas. J. Volcanol. Geotherm. Res. 110, 265–280.

Danyushevsky, L.V., Plechov, P., 2011. Petrolog3: integrated software for modeling crystallization processes. Geochem. Geophys. Geosyst. 12, Q07021. doi:10.1029/2011GC003516.

Danyushevsky, L.V., Della-Pasqua, F.N., Sokolov, S., 2000. Re-equilibration of melt inclusions trapped by magnesian olivine phenocrysts from subduction-related magmas: petrological implications. Contrib. Mineral. Petrol. 138, 68–83. doi:10.1007/PL00007664.

Dauphas, N., Craddock, P.R., Asimow, P.D., Bennett, V.C., Nutman, A.P., Ohnenstetter, D., 2009. Iron isotopes may reveal the redox conditions of mantle melting from Archean to Present. Earth Planet. Sci. Lett. 288, 255–267. doi:10.1016/j.epsl.2009.09.029.

Dixon, J.E., Stolper, E., Holloway, J.R., 1995. An experimental study of water and carbon dioxide solubilities in mid-ocean ridge basaltic liquids. Part I: calibration and solubility models. J. Petrol. 36, 1607–1631.

Elburg, M.A., Kamenetsky, V.S., 2007. Dehydration processes determine fO2 of arc and intraplate magmas. Geochim. Cosmochim. Acta 71, A252.

Elliott, T., Plank, T., Zindler, A., White, W.M., Bourdon, B., 1997. Element transport from slab to volcanic front at the Mariana arc. J. Geophys. Res. 102, 14991–15019.

Evans, K.A., Tomkins, A.G., 2011. The relationship between subduction zone redox budget and arc magma fertility. Earth Planet. Sci. Lett. 308, 401–409. doi:10.1016/j.epsl.2011.06.009.

Frost, B.R., Ballhaus, C., 1998. Comment on "Constraints on the origin of the oxidation state of mantle overlying subduction zones: an example from Simcoe, Washington, USA" by A. D. Brandon and D. S. Draper. Geochim. Cosmochim. Acta 62, 329–331.

Gaetani, G.A., O'Leary, J.C., Shimizu, N., Bucholz, C.E., 2010. Decoupling of H_2O, oxygen fugacity and incompatible elements in olivine-hosted melt inclusions by diffusive re-equilibration. EOS Transactions AGU, Abstract V23E-06.

Gill, J.B., 1981. Orogenic Andesites and Plate Tectonics. Springer-Verlag, New York.

Hauri, E.H., Gaetani, G.A., Green, T.H., 2006. Partitioning of water during melting of the Earth's upper mantle at H2O-undersaturated conditions. Earth Planet. Sci. Lett. 248, 715–734. doi:10.1016/j.epsl.2006.06.014.

Holloway, J.R., 2004. Redox reactions in seafloor basalts: possible insights into silicic hydrothermal systems. Chem. Geol. 210, 225–230. doi:10.1016/j.chemgeo.2004.06.009.

Irvine, T.N., Baragar, W.R.A., 1971. A Guide to the Chemical Classification of the Common Volcanic Rocks. Can. J. Earth Sci. 8, 523–548.

Jackson, C.M., Cottrell, E., Kelley, K.A., 2010. Mineral-melt partitioning of V and Sc at arcs: implications for mantle wedge oxygen fugacity. Presented at 2010 Fall Meeting, AGU, San Francisco, Calif., 13–17 Dec. Abstract V11F-01.

Jenner, F.E., O'Neill, H.S.C., Arculus, R.J., Mavrogenes, J.A., 2010. The magnetite crisis in the evolution of arc-related magmas and the initial concentration of Au, Ag and Cu. J. Petrol. 51, 2445–2464. doi:10.1093/petrology/egq063.

Johnson, M.C., Plank, T., 1999. Dehydration and melting experiments constrain the fate of subducted sediments. Geochem. Geophys. Geosyst. 1.

Jugo, P.J., Wilke, M., Botcharnikov, R.E., 2010. Sulfur K-edge XANES analysis of natural and synthetic basaltic glasses: implications for S speciation and S content as function of oxygen fugacity. Geochim. Cosmochim. Acta 74, 5926–5938. doi:10.1016/j.gca.2010.07.022.

Kelley, K.A., Cottrell, E., 2009. Water and the oxidation state of subduction zone magmas. Science 325, 605–607. doi:10.1126/science.1174156.

Kelley, K.A., Plank, T., Ludden, J.N., Staudigel, H., 2003. Composition of altered oceanic crust at ODP Sites 801 and 1149. Geochem. Geophys. Geosyst. 4. doi:10.1029/2002GC000435.

Kelley, K.A., Plank, T., Grove, T.L., Stolper, E.M., Newman, S., Hauri, E.H., 2006. Mantle melting as a function of water content beneath back-arc basins. J. Geophys. Res. 111, B09208. doi:10.1029/2005JB003732.

Kelley, K.A., Plank, T., Newman, S., Stolper, E., Grove, T.L., Parman, S., Hauri, E., 2010. Mantle melting as a function of water content beneath the Mariana arc. J. Petrol. 51, 1711–1738. doi:10.1093/petrology/egq036.

Kent, A.J.R., Elliott, T.R., 2002. Melt inclusions from Mariana arc lavas: implications for the composition and formation of island arc magmas. Chem. Geol. 183, 263–286.

Kessel, R., Schmidt, M.W., Ulmer, P., Pettke, T., 2005. Trace element signature of subduction-zone fluids, melts and supercritical liquids at 120–180 km depth. Nature 437, 724–727. doi:10.1038/nature03971.

Kress, V.C., Carmichael, I.S.E., 1991. The compressibility of silicate liquids containing Fe2O3 and the effect of composition, temperature, oxygen fugacity and pressure on their redox states. Contrib. Mineral. Petrol. 108, 82–92.

Lecuyer, C., Ricard, Y., 1999. Long-term fluxes and budget of ferric iron: implication for the redox states of the Earth's mantle and atmosphere. Earth Planet. Sci. Lett. 165, 197–211.

Lee, C.-T.A., Brandon, A.D., Norman, M.D., 2003. Vanadium in peridotites as a proxy for paleo-fO2 during partial melting: prospects, limitations, and implications. Geochim. Cosmochim. Acta 67, 3045–3064. doi:10.1016/S0016-7037(00)00268-0.

Lee, C.-T.A., Leeman, W.P., Canil, D., Li, Z.-X.A., 2005. Similar V/Sc systematics in MORB and arc basalts: implications for the oxygen fugacities of their mantle source regions. J. Petrol. 46, 2313–2336. doi:10.1093/petrology/egi056.

Lee, C.-T.A., Luffi, P., Plank, T., Dalton, H., Leeman, W.P., 2009. Constraints on the depths and temperatures of basaltic magma generation on Earth and other terrestrial planets using new thermobarometers. Earth Planet. Sci. Lett. 279, 20–33. doi:10.1016/j.epsl.2008.12.020.

Lee, C.-T.A., Luffi, P., Le Roux, V., Dasgupta, R., Albaréde, F., Leeman, W.P., 2010. The redox state of arc mantle using Zn/Fe systematics. Nature 468, 681–685. doi:10.1038/nature09617.

Mallmann, G., O'Neill, H.S.C., 2009. The crystal/melt partitioning of V during mantle melting as a function of oxygen fugacity compared with some other elements (Al, P, Ca, Sc, Ti, Cr, Fe, Ga, Y, Zr and Nb). J. Petrol. 50, 1765–1794. doi:10.1093/petrology/egp053.

Médard, E., Grove, T.L., 2007. The effect of H2O on the olivine liquidus of basaltic melts: experiments and thermodynamic models. Contrib. Mineral. Petrol. 155, 417–432. doi:10.1007/s00410-007-0250-4.

Métrich, N., Berry, A.J., O'Neill, H.S.C., Susini, J., 2009. The oxidation state of sulfur in synthetic and natural glasses determined by X-ray absorption spectroscopy. Geochim. Cosmochim. Acta 73, 2382–2399. doi:10.1016/j.gca.2009.01.025.

Miyashiro, A., 1974. Volcanic rock series in island arcs and active continental margins. Am. J. Sci. 274, 321–355.

Mungall, J.E., 2002. Roasting the mantle: slab melting and the genesis of major Au and Au-rich Cu deposits. Geology 30, 915–918.

Newman, S., Lowenstern, J.B., 2002. VolatileCalc: a silicate melt–H2O–CO2 solution model written in Visual Basic for excel. Comput. Geosci. 28, 597–604.

Nozaka, T., 2003. Compositional heterogeneity of olivine in thermally metamorphosed serpentinite from Southwest Japan. Am. Mineral. 88, 1377–1384.

Oppenheimer, C., 2003. Volcanic degassing, treatise on geochemistry. , pp. 123–166.

Parkinson, I.J., Arculus, R.J., 1999. The redox state of subduction zones: insights from arc-peridotites. Chem. Geol. 160, 409–423.

Pearce, J., Parkinson, I.J., 1993. Trace element models for mantle melting: application to volcanic arc petrogenesis. In: Prichard, H.M., Alabaster, T., Harris, N.B.W., Nears, C.R. (Eds.), Magmatic Processes and Plate Tectonics, pp. 373–403.

Pearce, J., Stern, R.J., 2006. The origin of back-arc basin magmas: trace element and isotope perspectives. In: Christie, D.M., Fisher, C.R. (Eds.), Back-arc Spreading Systems: Geological, Biological, Chemical, and Physical Interactions. American Geophysical Union, Washington, DC, pp. 63–86.

Plank, T., 2005. Constriants from Thorium/Lanthanum on sediment recycling at subduction zones and the evolution of the continents. J. Petrol.. doi:10.1093/petrology/egi005

Plank, T., Langmuir, C.H., 1998. The chemical composition of subducting sediment and its consequences for the crust and mantle. Chem. Geol. 145, 325–394.

Putirka, K.D., Perfit, M., Ryerson, F.J., Jackson, M.G., 2007. Ambient and excess mantle temperatures, olivine thermometry, and active vs. passive upwelling. Chem. Geol. 241, 177–206. doi:10.1016/j.chemgeo.2007.01.014.

Saal, A.E., Hart, S.R., Shimizu, N., Hauri, E.H., Layne, G.D., 1998. Pb isotopic variability in melt inclusions from oceanic island basalts, Polynesia. Science 282, 1481–1484.

Schneider, M.E., Eggler, D.H., 1986. Fluids in equilibrium with peridotite minerals: implications for mantle metasomatism. Geochim. Cosmochim. Acta 50, 711–724. doi:10.1016/0016-7037(86)90347-9.

Shaw, A.M., Hauri, E.H., Fischer, T.P., Hilton, D.R., Kelley, K.A., 2008. Hydrogen isotopes in Mariana arc melt inclusions: implications for subduction dehydration and the deep-Earth water cycle. Earth Planet. Sci. Lett. 275, 138–145. doi:10.1016/j.epsl.2008.08.015.

Sisson, T.W., Layne, G.D., 1993. H_2O in basalt and basaltic andesite glass inclusions from four subduction-related volcanoes. Earth Planet. Sci. Lett. 117, 619–635.

Sobolev, A.V., Shimizu, N., 1993. Ultra-depleted primary melt included in an olivine from the Mid-Atlantic Ridge. Nature 363, 151–154.

Stern, R.J., Ito, E., 1983. Trace-element and isotopic constraints on the source of magmas in the active Volcano and Mariana island arcs, western Pacific. J. Volcanol. Geotherm. Res. 18, 461–482.

Stolper, E., Newman, S., 1994. The role of water in the petrogenesis of Mariana trough magmas. Earth Planet. Sci. Lett. 121, 293–325.

Wade, J.A., Plank, T., Melson, W.G., Soto, G.J., Hauri, E.H., 2006. The volatile content of magmas from Arenal volcano, Costa Rica. J. Volcanol. Geotherm. Res. 157, 94–120. doi:10.1016/j.jvolgeores.2006.03.045.

Wallace, P.J., 2005. Volatiles in subduction zone magmas: concentrations and fluxes based on melt inclusion and volcanic gas data. J. Volcanol. Geotherm. Res. 140, 217–240. doi:10.1016/j.jvolgeores.2004.07.023.

Wallace, P.J., Carmichael, I.S.E., 1994. S speciation in submarine basaltic glasses as determined by measurements of $SK\alpha$ X-ray wavelengths. Am. Mineral. 79, 161–167.

Webster, J.D., Botcharnikov, R.E., 2011. Distribution of sulfur between melt and fluid in S–O–H–C–Cl–bearing magmatic systems at shallow crustal pressures and temperatures. Rev. Mineral. Geochem. 73, 247–283. doi:10.2138/rmg.2011.73.9.

Wood, B.J., Bryndzia, L.T., Johnson, K.E., 1990. Mantle oxidation-state and its relationship to tectonic environment and fluid speciation. Science 248, 337–345.

Woodhead, J.D., 1988. The origin of geochemical variations in Mariana lavas: a general model for petrogenesis in intra-oceanic island arcs? J. Petrol. 29, 805–830.

Woodhead, J.D., 1989. Geochemistry of the Mariana arc (western Pacific): source composition and processes. Chem. Geol. 76, 1–24. doi:10.1016/0009-2541(89)90124-1.

Zimmer, M.M., Plank, T., Hauri, E.H., Yogodzinski, G.M., Stelling, P., Larsen, J., Singer, B., Jicha, B., Mandeville, C., Nye, C.J., 2010. The role of water in generating the calc-alkaline trend: new volatile data for aleutian magmas and a new tholeiitic index. J. Petrol. 51, 2411–2444. doi:10.1093/petrology/egq062.